JOURNAL OF OPTOELECTRONICS AND ADVANCED MATERIALS Vol. 8, No. 5, October 2006, p. 1698 - 1702

Surface magnetic behavior and microstructures of ferromagnetic $(Co_{77}Si_{13.5}B_{9.5})_{90}Fe_7Nb_3$ ribbons

L. FERNÁNDEZ[a*], A. CHIZHIK[a], N. ITURRIZA[a], J.J.DEL VAL[a,b], J. GONZÁLEZ[a]
[a] *Física de Materiales, Fac. de Química. University of the Basque Country (UPV/EHU), San Sebastian, Spain.*
[b] *Unidad de Física de Materiales, Centro Mixto CSIC-UPV/EHU, San Sebastian, Spain.*

Different kinds of magnetic anisotropies have been induced during the nanocrystallization process of Co-rich amorphous ferromagnetic (*Finemet*) ribbons ($(Co_{77}Si_{13.5}B_{9.5})_{90}Fe_7Nb_3$) using diverse procedures like the application of a constant stress or an axial magnetic field during the annealing process. Magnetization measurements of the samples by a fluxmetric method in quasistatic conditions have evidenced the anisotropy of the treated *Finemet* samples. The main goal of this work has been the structural and microstructural analysis of the treated ribbons using X-ray Diffraction and Atomic Force Microscopy (AFM), detecting substantial differences in the crystallization state and grain size of the samples depending on the treatment that was carried out. Moreover, AFM measurements revealed in all the treated samples a strong nanocrystallisation of the surface without evidences of amorphous matrix, which contrast with Transmission Electron Microscopy measurements that have shown a high content of amorphous phase in the bulk of the ribbons. Additionally, magneto-optical Kerr effect measurements have been performed with the aim to elucidate the complex magnetic behavior that is expected for the surface of the ribbons, measuring surface hysteresis loops that show much higher coercive field values than in the bulk.

(Received September 5, 2006; accepted September 13, 2006)

Keywords: Finemet, Nanocrystallization, Induced anisotropy

1. Introduction

Soft ferromagnetic nanocrystalline alloys with trademark *Finemet* reveal superior soft magnetic properties as consequence of their microstructure, composed of an ultrafine grain structure of bcc Fe-Si grains with typical sizes around 10-15 nm embedded in an amorphous matrix. The grains are produced by devitrification of the amorphous Fe-Cu-Nb-Si–B alloy after thermal treatment, being the reduced grain size compared with the ferromagnetic correlation length (35 nm) the key for the extremely low effective magnetocrystalline anisotropy of these materials. This fact leads to small coercivity (around 1 A/m), and high initial permeability values, which are decisive factors that, together with their mechanical properties and their resistance to corrosion, have triggered enormous interest in both scientific and industrial community. Important works have been performed by the controlled introduction of several anisotropies in the amorphous alloys in order to tailor the shape of the hysteresis loops according to the demand of the technical applications. It should be considered that in these materials a small induced anisotropy can be of relative importance, because there is practically not magnetocrystalline anisotropy to compete against it. Several procedures, like the application of magnetic field or tensile stress during thermal treatment of the amorphous alloy are commonly used for the induction of anisotropy in the samples. In the case of magnetic field annealing, it is induced an uniaxial anisotropy where the easy axis is given by the direction of the applied magnetic field. This behavior has been explained by some authors in terms of thermally activated local atomic movements below the Curie temperature, taking place a directional-ordering process [1]. This phenomenon is the so-called "atomic pair ordering" that, in case of nanocrystallized alloys, is thought to occur mainly in the Fe-Si grains [2,3]. The field annealed samples show slightly smaller coercivity than the samples treated without field. On the other hand, the introduction of anisotropy by the application of a tensile stress induces an easy axis perpendicular to the applied stress. Two possible microstructural mechanisms try to explain the experimentally observed induced anisotropy: the first is the inelastic deformation of the amorphous matrix which creates internal stresses in the two-phase material [4], and the second one is an atomic rearrangement with more bonds oriented in the direction perpendicular to the axis of the applied stress than along this axis [5]. The induced anisotropy by tensile stress is found to be several orders of magnitude higher than the one induced by field annealing [6]. So far, multiple works dealing with the effects of the induced anisotropies on the magnetic properties of the nanocrystalline ribbons have been published. However, the microstructural or magnetic state of the surface of the ribbons stays completely unexplored. In the present work, the grain nucleation and growth mechanism in the bulk and at the surface of Co-rich *Finemet* alloys ($(Co_{77}Si_{13.5}B_{9.5})_{90}Fe_7Nb_3$) under the application of a magnetic field or a constant tensile stress during thermal treatment is studied. A structural analysis has been performed by X-ray diffraction (XRD), providing

information about the crystallization state in the bulk of the ribbons and the size of the grown nanocrystals, while Atomic Force Microscopy (AFM) has been used with the aim to elucidate the crystallization state in the surface of the ribbons. Finally, magneto-optical Kerr effect measurements have been carried out.

2. Experimental

2.1. Sample treatments

Amorphous ribbons, with the nominal composition mentioned above, were prepared by melt-spinning technique with dimensions: 3.1 mm wide and 20 μm thick. The amorphous character of the as-cast ribbons was confirmed by both XRD and TEM analysis. It was found that thermally treated ribbons show the formation of bcc-(Fe, Co[Si]) and fcc-Co phases [7]. The thermal treatments on the as-cast ribbons were carried out in air by Joule-heating. All the samples were submitted to the same annealing time (120 sec.) and current (32.9 A/mm^2), applying simultaneously an external tensile stress (500 MPa), or an axial magnetic field (750 A/m) during annealing and cooling down process to room temperature. The sample treated with stress will be identified as sample SA, and the one treated with magnetic field will be called FA. A third sample (CA) was submitted to the same annealing process with the application of neither an external magnetic field nor an external tensile stress. This ribbon was used as reference for the SA sample. Fluxmetric measurements carried out on the treated samples have evidenced the presence of an induced anisotropy, revealing completely different hysteresis loops depending on treatment [6].

2.2. Structural and microstructural analysis

As it was commented before, the structural analysis of *Finemet* ribbons was carried out by XRD, and additionally AFM measurements in tapping mode to analyze the surface of the ribbons. XRD patterns have been normalized in the high *q*-range where the intensity cannot vary between the different samples owing to the very short structural distances responsible for the scattering in this *q* region. In the case of crystallized samples, the evaluation of the crystalline phase has been performed by the subtraction of the amorphous halo of the as-cast sample (*Ia*) to the measurement performed on the crystallized ribbon (*I*). The resulted intensity pattern can be used to estimate the crystallinity ratio, χ, which is defined as following:

$$\chi = \frac{\int q^2 (I - Ia) dq}{\int q^2 I dq} \qquad q = \frac{4\pi \sin\theta}{\lambda}$$

where (*I - Ia)* denotes the resulting intensity pattern that corresponds to the crystalline fraction of the sample, *q* is the scattering vector and 2θ is the scattering angle. Additionally, the crystallite size, *D*, has been evaluated from the Scherrer's formula.

3. Results and discussion

Usually, the X-ray reflexions of the amorphous ribbon become higher and narrower with longer time and temperature treatments, indicating the beginning of the crystallization process. Differences in the diffraction patterns of the treated samples are detected depending on the kind of annealing process that has been performed. In the following sections the analysis of the samples annealed with stress (SA) or with magnetic field (FA) will be separately exposed.

3.1. Stress annealing process

The XRD pattern corresponding to the sample SA presents an incipient but remarkable crystalline peak corresponding to the crystallization of the bcc-(Fe,Co[Si]) phase that is overlapped with the amorphous halo of the still present amorphous matrix. Fig. 1a discloses XRD patterns of sample SA, and the as-cast ribbon. The scattering excess in the XRD patterns of SA is an indication of crystallization, well fitted by a Gaussian function. From the analysis of the crystalline peak, a crystalline volume of 6% and grain size of 8.8 nm are obtained. The resulting grain size of 8.8 nm in the ribbon SA results to be relatively small compared to the typical grain size (10-15 nm) found in *Finemet* alloys after conventional thermal annealing, and it is thought to be linked with the application of a tensile stress during the annealing process due to modifications in the grain nucleation, which could avoid the growth of the grains to larger sizes. Similar results of small grain sizes (approx. 8 nm) have been also obtained by other authors using flash-stress annealing on *Finemet* ribbons [8]. Such modification in the grain nucleation of sample SA is detected in the comparison between the XRD patterns of samples SA and CA. While the XRD pattern of sample SA displays an incipient crystallization peak, the pattern of sample CA does not show any sign of crystallization following a Lorentz function, similar to the amorphous halo of the as cast ribbon of Fig. 1a. Therefore, it seems that the use of stress annealing enhance the nanocrystallization of *Finemet* ribbons.

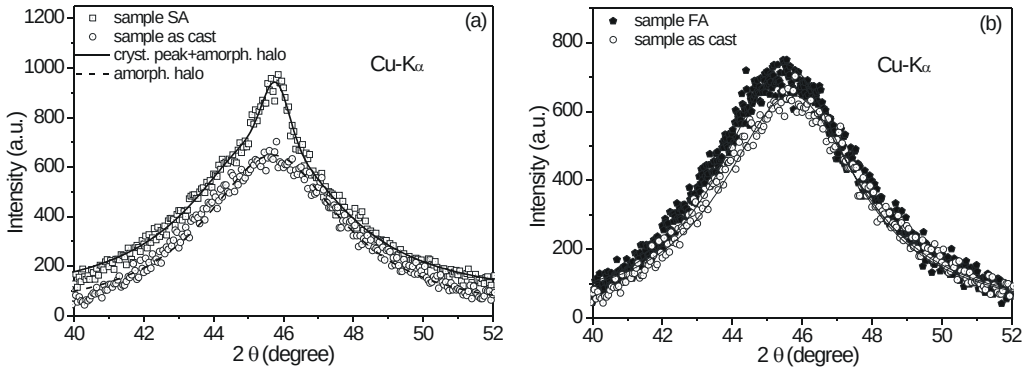

Fig. 1. XRD patterns for: (a) SA and as cast samples. The dash fitting line corresponds to a Lorentz function representing the amorphous halo of the XRD patterns. The solid one corresponds to a sum of a Gaussian (crystalline) and Lorentz function; and (b) FA and as cast samples. The lines are represented to help the view.

The AFM analysis of the ribbon surface shows a strong crystallization without signs of amorphous matrix. The nanograins are visible with a typical diameter of 9.3 nm (Fig. 2). The difference between the grain size obtained by XRD and by AFM can be explained taking into account that the AFM tip has a finite curvature that limits the lateral resolution for the measurement of objects with sizes very close to the nm scale in *x* and *y* directions. Such strong surface crystallization contrasts with the low 6% of crystalline volume obtained by XRD in sample SA, showing that the kinetic of grains nucleation and growth at the surface of the ribbons is completely different to the process that takes place in the bulk. These different crystallization states could be explained considering the higher energy of the surface that leads to a stronger instability of the surface morphology, resulting in an earlier crystallization than in the bulk.

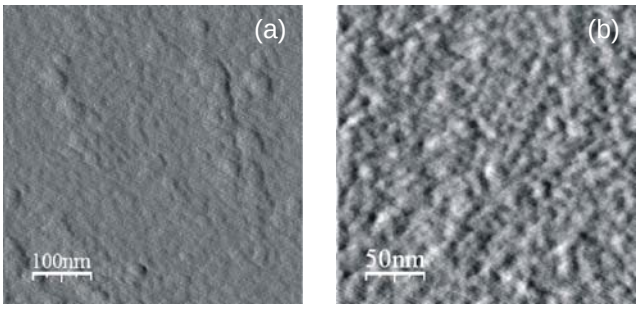

Fig. 2. AFM micrographs of the ribbon surface corresponding to sample SA. The micrographs are AFM phase images.

3.2. Field annealing process

The XRD measurements corresponding to sample FA show the absence of crystallization. Fig. 1b discloses the XRD patterns of the sample FA and the as-cast ribbon. The scattering excess of the measurement of the sample FA is a sign of structural relaxation or other possible mechanism like an incipient nucleation. The "quasi amorphous" state detected in the bulk of the ribbon contrasts with the AFM micrographs measured on the surface of the sample FA, which display a crystallized surface with typical grain sizes around 20 nm. Furthermore, the AFM micrographs of this sample present the formation of large agglomerates similar to inlands with typical sizes of approx. 125 nm that are locally arranged with an apparent ordering. This phenomenon could suggest an organization of these inlands at the surface of the ribbon during the thermal treatment under the effect of the applied magnetic field (Fig. 3). To analyze more in detail if the grown inlands present some periodicity in their arrangement, a special filter called "self-correlation" [9] was applied to the micrograph displayed in Fig. 3b. The result is a new image with an apparent periodicity (see Fig. 4) that could proof the periodicity in the arrangement of the inlands in the surface of sample FA. This fact could enforce the hypothesis of a self-organized growth of the inlands on the surface of the ribbons after the application of a magnetic field during the annealing process.

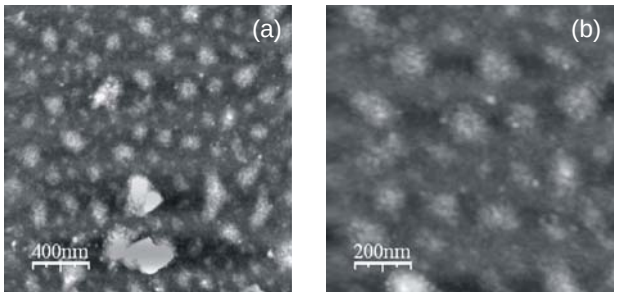

Fig. 3. AFM micrographs of the ribbon surface corresponding to sample FA at different magnifications.

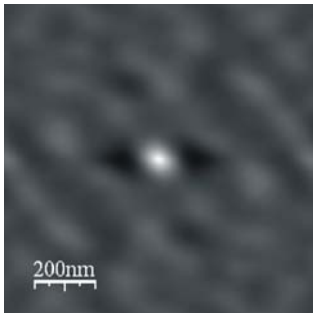

Fig. 4. "Self-correlation" filtered image of the original AFM micrograph (Fig. 3a).

3.3 Magneto-optical Kerr-effect measurements

Surface hysteresis loops were measured on samples FA and SA by magneto-optical Kerr effect. For this purpose an AC axial magnetic field (f =60 Hz) was applied to the sample, while a polarized light produced by a He-Ne laser was focused on the ribbon surface. The applied magnetic field and the laser light were aligned; therefore the rotation of the polarization plane of the reflected light was proportional to the magnetization, which is in the plane of the surface and parallel to the plane of the incident light. This is the so called longitudinal Kerr effect. Several measurements were carried out on the *Finemet* ribbons keeping magnetic field and laser light positions, but rotating the sample 180º in the plane with steps of 20º. The measured surface hysteresis loops display clear differences depending on the orientation of the ribbon respect to the applied magnetic field, which indicates anisotropy. In the case of sample SA, strong differences are found in the surface hysteresis loops measured in geometries where the magnetic field was applied parallel (orientation of 0º), or perpendicular to the axis of the ribbon (orientation of 90º). For an orientation of 0º, the surface hysteresis loops behave similarly to the bulk hysteresis loop of SA showing a clear inclined shape. Moreover, it was not possible to saturate in this geometry the surface hysteresis loops with the application of the maximum magnetic field available in the experimental set up. On the other hand, for an orientation of 90º the strong inclination commented before is not detected, and it is possible to saturate the surface hysteresis loop (see fig. 5a). This fact proves the presence of an induced easy axis transverse to the axis of the ribbon. For directions different of 90º or 0º the surface hysteresis loops are generally not saturated, and show an inclination that varies depending of the proximity to the orientation of 0º. Interesting remarks are the jumps found in the hysteresis loop at 90º orientation, which reveals the possible presence of two different, soft and hard, ferromagnetic phases in the ribbon surface. The surface hysteresis loops measured on sample FA show a behavior that is not expected, because an induced easy axis at an orientation of 30º respect to the ribbon axis is detected (Fig. 5b). Hysteresis loops, measured at angles around this direction (at 0º and 50º), show an abrupt change of behavior compared to the measurements at 30º. This result contrasts with the result obtained in previous bulk measurements, where the easy axis is oriented along the axis of the ribbon at 0º. The existence of an easy axis that is 30º disoriented respect to the ribbon axis could be assumed considering the effects of the magnetic field induced by the annealing current that could interact with the applied magnetic field during annealing treatment, turning aside its initial orientation. Consequently, an easy axis at 30º could be induced. Additionally, the surface hysteresis loop measurements reveal a magnetic hardening of the ribbon surface respect to the bulk, which is evidenced in the coercive values detected in these measurements that for both samples SA and FA are approx. 800-900 A/m.

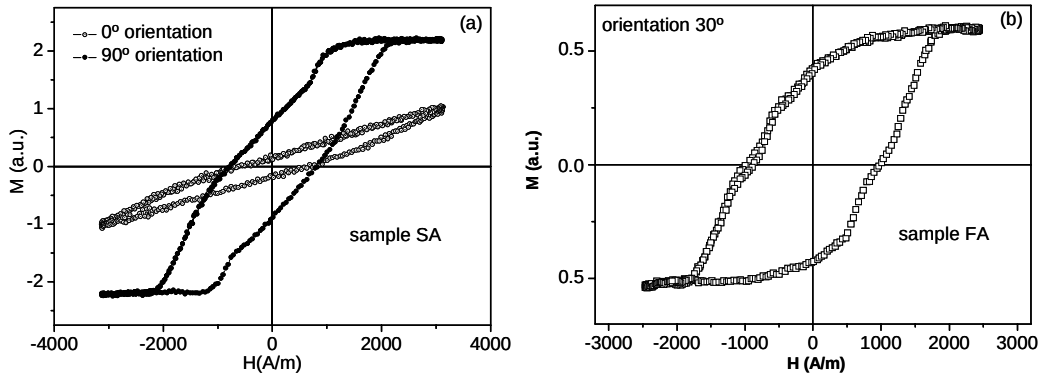

Fig. 5. Surface hysteresis loops measured by Kerr-effect on: (a) sample SA rotated 90º and 0º in the plane; and (b) on sample FA rotated 30º in the plane.

4. Conclusions

The application of a tensile stress or a magnetic field during thermal annealing of Co-rich *Finemet* ribbons is a well known technique to induce anisotropy in *Finemet* ribbons. In the present work, clear differences have been found in the grain growth mechanisms and crystallization of the bulk and surface of the ribbons depending on the performed treatment. The use of a tensile stress is found to activate the nucleation rate, while grains with a reduced grain size compared to standard treated *Finemet* ribbons are found. On the other hand, the use of applied field during thermal annealing seems to produce a completely different effect that does not activate the grain growth in the bulk, but it produces ordered arrangements of grain agglomerates at the surface of the ribbon, showing similarities with phenomena of self-organization. Additionally, surface hysteresis loops evidence the presence of anisotropies at the surface of the ribbons. In the case of sample SA is transverse to the ribbon axis, as it is expected. Nevertheless, the measurement carried out on sample FA shows an easy axis 30º oriented respect to the expected induced easy axis. Moreover, a strong hardening of the ribbon surface is detected compared to the bulk,

which could be explained considering the high density of inhomogeneities present at the surface that difficult the movement of the magnetic domains.

Acknowledgments

The authors acknowledge the financial support to the Department of Education of Eusko Jaurlaritza and by the Ministerio de Educación y Ciencia (MAT2004-05348-C04-04).

References

[1] B. S. Berry, W. C. Pritchet. Phys. Rev. Lett. **34** 1022 (1975).
[2] G. Herzer. Scripta Metallurgica et Materialia, **33**, 1741 (1995).
[3] J. González, O. Chubykalo, J.M. González. Enciclopedia of Nanoscience and Nanotechnology 10, 1-26 (2004).
[4] G. Herzer, IEEE Trans Magn. **5**, 1388 (1994).
[5] Y. Suzuki, J. Haimovich, T. Egami. Phys. Rev. B. **35,** 35 (1987).
[6] C. Miguel, A. P. Zhukov, J. J. Del Val, A. Ramirez de Arellano, J. González, J. Appl. Phys. **97**, 034911 (2005).
[7] N. Iturriza, L. Fernández, J. J. del Val, N. Murillo and J. González, to be published.
[8] F. Alves. J. Magn. Magn. Mat. **226-230**, 1490 (2001).
[9] Scanning microscope software WSxM. Program developed by Nanotec Electrónica S.L. (Spain).

*Corresponding author: wapvaalj@sq.ehu.es